Relativistic laser channeling in plasmas for fast ignition

A. L. Lei,[1,2,8,*] A. Pukhov,[3] R. Kodama,[1,2] T. Yabuuchi,[1,2] K. Adumi,[1,2] K. Endo,[1,2] R. R. Freeman,[4] H. Habara,[1,2] Y. Kitagawa,[1] K. Kondo,[1,2] G. R. Kumar,[5] T. Matsuoka,[1,2] K. Mima,[1] H. Nagatomo,[1] T. Norimatsu,[1] O. Shorokhov,[3] R. Snavely,[6] X. Q. Yang,[8] J. Zheng,[7] and K. A. Tanaka[1,2]

[1]*Institute of Laser Engineering, Osaka University, Suita, Osaka 565-0871, Japan*

[2]*Graduate School of Engineering, Osaka University, Suita, Osaka 565-0871, Japan*

[3]*Institut fur Theoretische Physik I, Heinrich-Heine-Universitat Duesseldorf, Duesseldorf 40225, Germany*

[4]*College of Mathematical and Physical Sciences, Ohio State University, Columbus, Ohio 43210, USA*

[5]*Tata Institute of Fundamental Research, Mumbai 400005, India*

[6]*Lawrence Livermore National Laboratory, University of California, Livermore, California 94550, USA*

[7]*Department of Modern Physics, University of Science and Technology of China, Hefei, Anhui 230026, China*

[8]*Shanghai Institute of Optics and Fine Mechanics, Chinese Academy of Sciences, Shanghai 201800, China*

(Received 3 March 2006; revised manuscript received 17 September 2007; published 18 December 2007)

We report an experimental observation suggesting plasma channel formation by focusing a relativistic laser pulse into a long-scale-length preformed plasma. The channel direction coincides with the laser axis. Laser light transmittance measurement indicates laser channeling into the high-density plasma with relativistic self-focusing. A three-dimensional particle-in-cell simulation reproduces the plasma channel and reveals that the collimated hot-electron beam is generated along the laser axis in the laser channeling. These findings hold the promising possibility of fast heating a dense fuel plasma with a relativistic laser pulse.

DOI: 10.1103/PhysRevE.76.066403 PACS number(s): 52.57.Kk, 52.38.Hb, 52.38.Kd

Exploration of the behavior of matter in extraordinarily large light fields is a new frontier in light-matter interaction studies [1]. The subject continues to grow at an explosive pace, and not only new physics, but many attractive applications are beginning to emerge. For example, energetic particles, such as hot electrons and fast protons and ions, can be generated in these interactions. These particle sources have many potential applications such as tabletop particle acceleration. A promising application of high-energy electrons is the fast ignition (FI) scheme, which is expected as a fast-track realization of inertial confinement fusion [2]. In the FI scheme, a compressed plasma core is heated to trigger a nuclear-fusion burn wave by hot electrons generated in the relativistic laser plasma interaction. One of the critical physics issues in the FI scheme is relativistic laser energy transport into the compressed core plasma from the long-scale-length coronal plasma. The popular idea is to use a physical reentrant cone to preclude the coronal plasma from the path of the relativistic laser beam, allowing the laser energy to be deposited close enough to the fuel core plasma [3]. An alternative idea is to inject the relativistic laser light directly into the corona plasma. This approach requires the relativistic laser pulse to channel into the dense fuel through large underdense and overdense plasmas.

Relativistic laser channeling in underdense and overdense plasmas has been explored both computationally and experimentally [4–15], where different plasma density profiles, laser powers, and timings between the laser pulses for preformed plasma creation and channeling have been considered. The intense laser pulse may undergo relativistic self-focusing in underdense plasmas [4] and propagate in overdense plasmas via relativistic induced transparency (RIT) [5] and laser hole boring (LHB) [6]. Complex nonlinear processes are involved in relativistic laser-plasma interactions, such as laser beam breakup [8] and propagation instabilities [9]. Technically, the laser-channeling phenomenon in an overdense plasma makes the measurement difficult. Hence, relativistic laser channeling in a plasma consisting of both extended underdense and overdense regions has not been yet observed. Here we report an indication of relativistic self-focused laser channeling into a high-density plasma.

The laser channeling experimental setup is shown in Fig. 1. A long GXII laser pulse ($\lambda=0.527$ μm, $\tau_{\mathrm{FWHM}}=1.3$ ns with Gaussian temporal profile $E_{\mathrm{long}}=40-48$ J) was focused through a random phase plate (RPP) [16] onto a 1-μm-thick deuterated carbon (CD) target with 0.1-μm-thick Al coating on the front surface to generate the preformed plasma. At 0.15 ns, after the peak of the GXII laser, the short-pulse GXII PW (PW) laser ($\lambda=1.053$ μm, $\tau=0.6$ ps, $E_{\mathrm{short}}=150-250$ J) was focused onto the preformed plasma from the same side as the GXII laser. The focus spot sizes [full width at half maximum (FWHM)] of the GXII and PW lasers were about 500 and 70 μm, respectively. The time-integrated keV x-ray images were obtained with a charge-

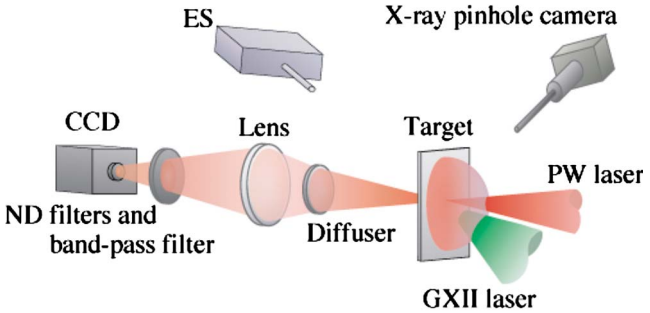

FIG. 1. (Color online) Experimental setup.

*lal@siom.ac.cn

coupled device- (CCD-) backed x-ray pinhole camera (XPHC) placed in front of the target at 21° to the PW laser axis. The distances from the target (target chamber center) to the pinhole and from the pinhole to the CCD camera were 117 mm and 1010 mm, respectively, giving a XPHC magnification of about 8.6. The XPHC had a 18-μm pinhole blocked with a 40-μm-thick Be filter. The transmitted PW laser light through the preformed plasma was measured via an imaging system consisting of an optical diffuser placed behind the target. The image of the diffuser was relayed onto an optical CCD through calibrated neutral-density (ND) and bandpass filters. Hot-electron energy spectra in the 1–100-MeV range were obtained with an electron spectrometer (ES) [17] placed behind the target at 21° to the PW laser axis.

Time-integrated XPHC images from the preformed plasmas with and without the PW laser interactions are shown in Figs. 2(a) and 2(b) and Fig. 2(c), respectively, as indicated by the energy values of the GXII laser, E_{long}, and the PW laser, E_{short}. The x-ray intensity profiles along the vertical dashed red lines in the images were added at the left side of the images. The preformed plasma shown in Fig. 2(a) had about a 500-μm-thick underdense region (from $0.1n_c$ to $1n_c$) and about a 80-μm-thick overdense region with a peak density of about $10n_c$ at the timing of the PW laser interaction, as shown in Fig. 2(d), based on the simulation by the one dimensional (1D) hydrodynamic code ILESTA_1D [18]. Here n_c is the plasma critical density. The code ILESTA_1D was benchmarked for a similar preformed plasma by x-ray and ultraviolet laser probe diagnostics [19] and was used to prepare the overdense plasma. The plasma density is $0.86n_c$ at the PW laser focus point (80 μm behind the target surface in the experiment). The large ellipse in Fig. 2(a) is due to the GXII laser irradiation on the target, corresponding to the preformed plasma. The most striking feature in Fig. 2(a) is that there is an elongated region at the center of the ellipse from where the x-ray emission is considerably weaker than in the surrounding region, as indicated in the x-ray intensity profile of Fig. 2(a). This elongated region can be interpreted as due to the presence of a plasma channel. Another plasma channel was reproduced in the XPHC image when changing the PW laser focus point to $0.6n_c$ (20 μm behind the target surface in the experiment), as shown in Fig. 2(b). There are also small fluctuations in the x-ray intensity profiles of Figs. 2(a) and 2(b), which might be caused by the RPP effect. There was no such channel formation observed when only the GXII laser irradiated the target, as shown in Fig. 2(c). These two observations indicate PW laser channeling in the preformed plasma.

In Figs. 2(a) and 2(b), one sees that the direction of both plasma channels coincides with the PW laser axis, indicating that the pointing of the PW laser channeling in the preformed plasmas is reproducible and along the laser axis. The PW laser beam pointing is a crucial issue for FI. One of the necessary conditions for FI is the generation of a collimated hot-electron beam along the PW laser axis toward the compressed tiny core plasma for efficient heating. If the PW laser and the generated hot electrons miss the core plasma, then the electron beam cannot initiate a hot spark and thermonuclear burn propagation. The PW laser must propagate in the plasma along its axis in an integrated FI experiment.

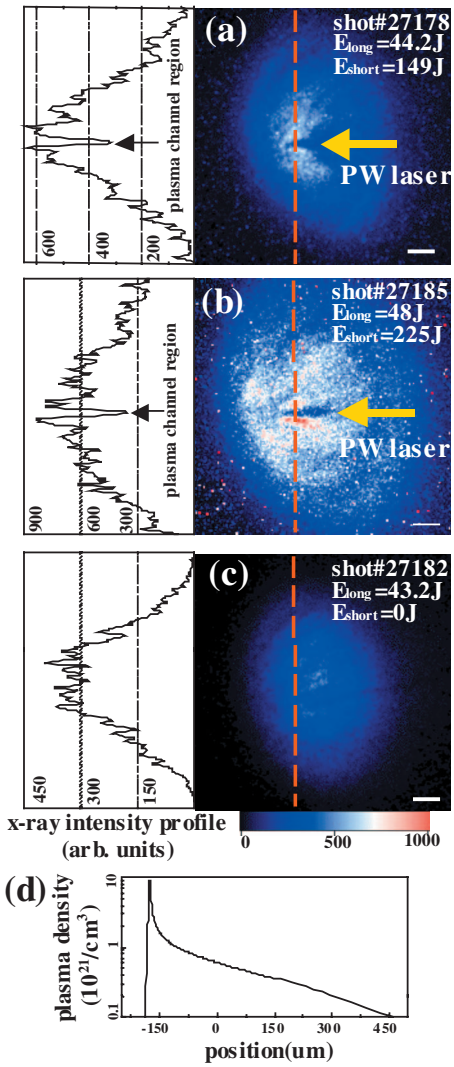

FIG. 2. (Color) Time-integrated x-ray pinhole camera images from the preformed plasmas taken (a),(b) with and (c) without the PW laser interactions. (d) is the simulated plasma density profile at the timing of the PW laser interaction for (a). In (d), the position at 0 μm corresponds to the target surface. The PW laser was focused at position −80 μm (i.e., 80 μm behind the target surface) for (a) in the experiment. The x-ray intensity profiles along the vertical dashed red lines in the images (a)–(c) are added at the left side of the images. E_{long} and E_{short} denote the energies of the long-pulse GXII laser and the short-pulse PW laser. The color codes are in arbitrary units. The white scale bars correspond to 100 μm. Note that the real plasma channel lengths should be 2.79 (=1/sin 21°) times the channel lengths shown in (a) and (b) since the XPHC was placed not at 90°, but at 21° to the PW laser axis.

The observed channel regions shown in Figs. 2(a) and 2(b) are created by the strong ponderomotive force of the PW laser pulse. This force pushes the electrons and subsequently ions out of the channel, leading to the depletion of electrons and ions in the channel region. We note that the XPHC images shown in Figs. 2(a) and 2(b) do not reflect plasma channel formation at the timing of the PW laser interaction, because the images are time integrated and the plasma structure changes in time. After the passage of the PW laser pulse, the plasma channel is created and then ex-

pands radially. An earlier experiment showed that the plasma channel can last at least of the order of several 100 ps [15].

We now discuss how the elongated region with weaker x-ray emission in Figs. 2(a) and 2(b) is related to the plasma channel. First, although the PW laser energy is locally converted into the multi-MeV hot electrons in the channel region, the hot electrons may not be responsible for heating locally the channel wall and background plasma, but rather responsible for heating the whole plasma due to their long mean free path, consistent with the higher background x-ray level in Figs. 2(a) and 2(b) than in Fig. 2(c). Such nonlocal heating has been observed with four shots in an earlier campaign months before the present run. In the earlier campaign, the PW laser irradiated the preformed plasmas (created with 3.2-μm-thick CD foils) at 0.88 ns after the peak of the GXII laser (i.e., after the GXII laser) and no relatively enhanced keV x-ray emission along the PW laser axis was observed, indicating that the whole plasma was heated by hot electrons generated by the PW laser pulse. In the present experiment, the GXII laser energy was kept nearly same (40–48 J), the large difference in background x-ray emission intensities between Figs. 2(a) and 2(b) and Fig. 2(c) indicating that the plasma temperatures are increased due to the heating of the whole plasmas by the PW laser pulse, provided that the x-ray emission is inverse bremsstrahlung. It is also shown that the background x-ray level is higher in Fig. 2(b) than in Fig. 2(a) due to the relatively larger PW laser energy in Fig. 2(b). Second, the GXII laser heating causes relatively weaker x-ray emission from the plasma channel region. The electrons and ions in the plasma channel are expelled into the surrounding plasma region by the PW laser pulse and the radially expanding plasma channel will be depleted of electrons and ions. After the PW laser passage and the plasma channel formation, the GXII laser still irradiated the whole plasma for several 100 ps. The plasma channel with depleted electrons and ions therefore has less x-ray emission than other plasma regions, leading to the contrast of x-ray intensity on the XPHC images shown as the elongated region with weaker x-ray emission.

The x-ray pictures showing a plasma channel formation in Figs 2(a) and 2(b) could be reconstructed with an analytical processing taking into account inverse bremsstrahlung x-ray emission and absorption with given plasma parameters. A full discussion of the reconstruction will be presented elsewhere [20]. We consider that the x-ray emission is inverse bremsstrahlung that depends on the plasma density $n_e(x,y,z)$ and temperature $T_e(x,y,z)$ distributions. We performed a 2D hydrodynamic simulation for the 1.3-ns-long pulse GXII laser with laser and target parameters the same as the experimental ones to give the 2D plasma density $n_e(x,y)$ and temperature $T_e(x,y)$ profiles, from which we can obtain the 3D $n_e(x,y,z)$ and $T_e(x,y,z)$ by assuming that the plasma density and temperature profiles are symmetrical relative to the plasma channel axis. We did not consider modification of the plasma temperature by the short-pulse PW laser heating since the particle-in-cell (PIC) code cannot accurately give the plasma temperature value. The modification of the plasma density due to PW laser channeling was considered, and the plasma density profile at the timing of the PW laser

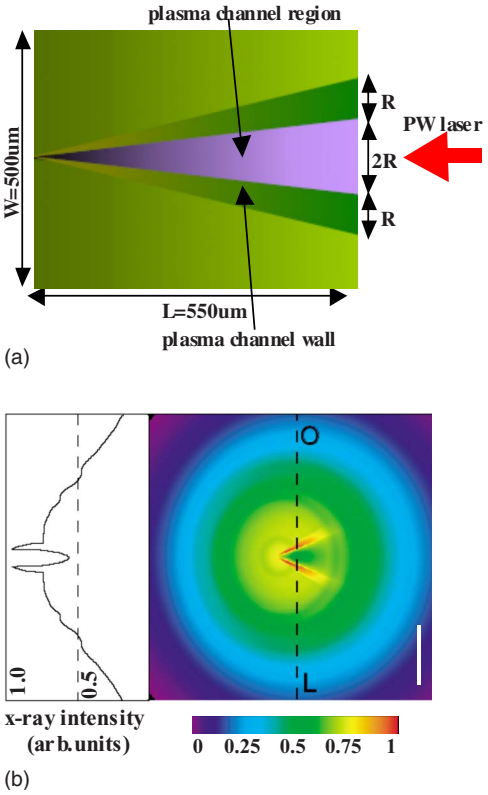

FIG. 3. (Color online) Reconstructed x-ray picture showing a plasma channel. (a) is the preformed plasma density distribution. The plasma channel in (a) is assumed to have a cone shape with $L/2R=4$. (b) is the reconstructed x-ray pinhole picture for (a). The x-ray intensity profile along the dashed OL line in the image (b) is added at the left side of the image. The white scale bar in (b) corresponds to 100 μm.

interaction was assumed as shown in Fig. 3(a). The plasma channel had a cone shape. The density at the cone tip was the simulated peak density. The density outside the channel region was $n_e(x,y)$, which was given by the 2D hydrodynamic simulation, and the density inside the channel region was $0.1n_e(x,y)$, which was assumed according to the PIC simulation [7]. The density inside the channel wall was estimated to be $2-3n_e(x,y)$, assuming all expelled electrons at the channel region are pushed into the channel wall. The inverse bremsstrahlung keV x-ray emission was then calculated with the above estimated plasma density and temperature profiles at the timing of the PW laser interaction. The picture of the keV x-ray emission observed from a pinhole placed at 21° relative to the plasma channel axis is thus obtained, as shown in Fig. 3(b). A plasma channel is clearly seen. The reconstructed x-ray image [Fig. 3(b)] reproduces the main feature (plasma channel formation) of the experimental XPHC images shown in Figs. 2(a) and 2(b).

Figure 4(a) is the transmitted image through the focused region on an optical diffuser with a low-energy PW laser shot without any target as transmitted PW laser energy calibration. The image shows a near-field, ring feature pattern of the PW laser itself [21]. Figure 4(b) shows the diffuser image taken at the shot shown in Fig. 2(a). Note the measured light in Fig. 4(b) is due to the PW laser transmission through the

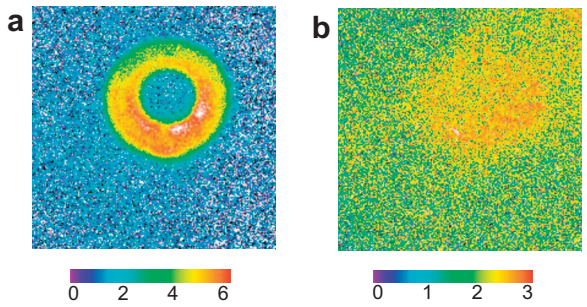

FIG. 4. (Color) Optical diffuser images. Transmitted PW laser light was observed on the diffuser. (a) 0.8-J PW laser energy for calibration and (b) 149-J PW laser energy. The color bar is in an exponential scale and in arbitrary unit.

preformed plasma, not due to the coherent transition radiation from the hot electrons generated by the PW laser pulse [22] where a solid-vacuum boundary at the target rear is necessary. The value of transmitted PW laser energy through the diffuser images was estimated to be 3.8%, indicating PW laser channeling through the high-density plasma. The PW laser channeling in overdense plasmas is due to both RIT and LHB, which are driven by the laser light ponderomotive pressure. The velocity of LHB is given by [6]

$$u = c\left(\frac{n_c}{2n_e}\frac{Zm_e}{M_0}\frac{I\lambda^2}{1.37\times 10^{18}}\right)^{1/2}, \tag{1}$$

where c is the speed of light, Z the effective ionic charge state, m_e and M_0 the electron and ion masses, I the laser intensity in $\mathrm{W/cm^2}$, and λ the laser wavelength in μm. The PW laser focus size in vacuum was about 70 μm. Taking into account both RIT and LHB for the simulated plasma density profile shown in Fig. 2(d) and using Eq. (1), we estimate that the PW laser should self-focus down to about 20 μm to penetrate through the preformed plasma for the observed transmission. This transmission together with the keV x-ray measurement shown in Fig. 2(a) indicates PW laser channeling through the overdense plasma along its axis with relativistic self-focusing. Changing the PW laser focus point to $0.6n_c$, however, only 6×10^{-5} of the transmitted PW laser energy was obtained, indicating that the PW laser channeling in the preformed plasma is strongly dependent on its focus position.

The measured hot-electron energy spectra showed electron temperatures ranging from 2.5 to 4.0 MeV, similar to the simulated value ~4.1 MeV.

We performed a 3D virtual laser plasma laboratory (VLPL) PIC simulation [23] to reproduce the plasma channel in the overdense plasma. The plasma has a density profile $n_e = 10n_c \exp(-x/L)$ with $L=40$ μm and $x=0-100$ μm, similar to the experimental one for the shot shown in Fig. 2(a). The channeling laser pulse has the Gaussian shape $a = a_0 \exp(-r^2/R^2)\exp(-t^2/\tau^2)$ with beam diameter $2R = 40$ μm and Gaussian temporal profile with peak power of 0.3 PW. Figures 5(a)–5(c) show the electron density and Figs. 5(e)–5(g) give the electromagnetic energy density distributions snapped at times $t/T=100$, 200, and 300, where $T=3.3$ fs is the laser period. One first observes the filamentation of the laser pulse [Figs. 5(a) and 5(e)]. Then, the filaments coalesce into a single channel [Figs. 5(b) and 5(f)]. This plasma channel continuously drills through the plasma layer up to $10n_c$ [Figs. 5(c) and 5(g)] and expands even after the laser pulse is over and finally punches through the whole plasma layer. In the simulation, the RIT and LHB processes dominate in the plasma channel formation at the beginning. When the laser pulse penetrates to $6n_c$, the hot electrons generated go forward faster than the laser pulse. These hot electrons force the local background electrons out of their path, thus aiding to form an electron-depleted plasma channel. The laser pulse is guided in the channel to propagate to the high-density plasma region. The hot electrons with energy more than 1 MeV are highly collimated around the laser axis, as shown in Fig. 5(d) where the hot-electron density distribution is snapped at the time of channel formation. The time corresponds to Figs. 5(b) and 5(f). This stable and on-axis behavior of hot electrons is different from the relativistic laser interactions with preplasmas created by the prepulse or pedestal of the laser itself on solid targets, where the hot-electron beam direction is neither stable nor along the laser axis [24,25]. Though both laser and electron behaviors are described in our condition by VLPL PIC simulations, the hot-electron energy transport in an initially cold, dense plasma stays as an important issue for future study [26]. The collimation of directional MeV hot electrons was also experimentally observed by focusing the PW laser into an im-

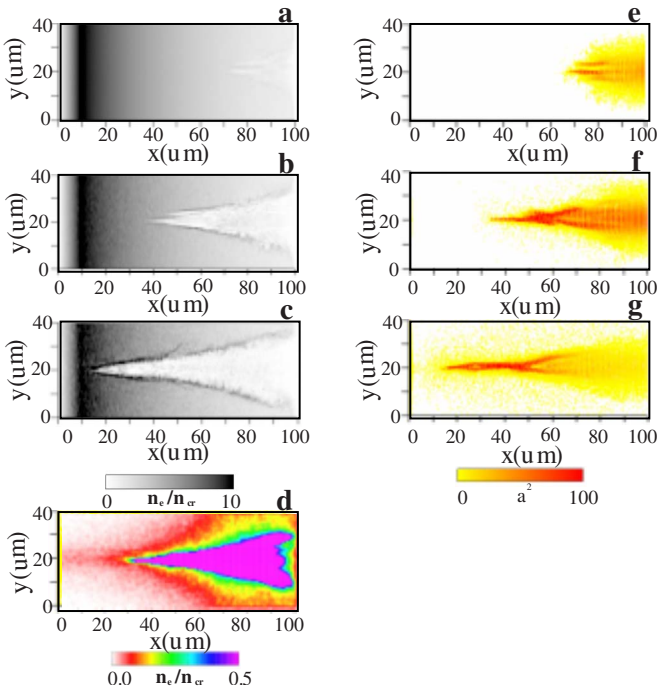

FIG. 5. (Color online) 3D particle-in-cell simulation results. (a)–(c) show the channel development in the plasma electron density at times $t/T=100$, 200, and 300. (e)–(g) show the relativistically normalized laser intensity $a^2=e^2(E^2+B^2)/(m_e c\omega)^2$, at times $t/T=100$, 200, and 300. (d) shows the hot-electron distribution at time $t/T=200$. The laser pulse filaments first appear [see (a) and (e)], and then the filaments coalesce and the conic channel is formed [see (b) and (f)]. This channel is guided by the collimated beam of laser-accelerated hot electrons as seen in (d).

ploded coronal plasma [27], a plasma with similar density profile for the shot shown in Fig. 2(a). We could expect that a highly directional and collimated MeV hot-electron beam was generated in our experimental condition where the PW laser channeled into the overdense plasma.

In summary, we experimentally and computationally investigated relativistic laser channeling in large-scale-length preformed plasmas. Our keV x-ray and laser light transmittance measurements suggest laser channeling along its axis through overdense plasmas with relativistic self-focusing. A three-dimensional PIC simulation reproduces the channel formation and indicates that the plasma channel and hot-electron flux could be generated along the relativistic laser axis in an imploded plasma for an integrated FI experiment. A highly directional and collimated hot-electron beam is expected to point toward the compressed tiny core plasma for rapid heating for FI.

We thank the ILE staff for the laser operation, target fabrication, and data acquisition. Part of this research is supported by the JSPS Japan-China Core University Program, the BRJH Program of CAS, and the Natural Sciences Foundation of China under Grant No. 10775165. A.L.L. acknowledges JSPS for support.

[1] M. D. Perry and G. Mourou, Science **264**, 917 (1994).
[2] M. Tabak *et al.*, Phys. Plasmas **1**, 1626 (1994).
[3] R. Kodama *et al.*, Nature (London) **412**, 798 (2001).
[4] A. B. Borisov *et al.*, Phys. Rev. Lett. **68**, 2309 (1992).
[5] V. A. Vshivkov *et al.*, Phys. Plasmas **5**, 2727 (1998).
[6] S. C. Wilks, W. L. Kruer, M. Tabak, and A. B. Langdon, Phys. Rev. Lett. **69**, 1383 (1992).
[7] A. Pukhov and J. Meyer-ter-Vehn, Phys. Rev. Lett. **79**, 2686 (1997).
[8] K. A. Tanaka *et al.*, Phys. Rev. E **62**, 2672 (2000).
[9] Z. Najmudin *et al.*, Phys. Plasmas **10**, 438 (2003).
[10] M. Borghesi, A. J. MacKinnon, L. Barringer, R. Gaillard, L. A. Gizzi, C. Meyer, O. Willi, A. Pukhov, and J. Meyer-ter-Vehn, Phys. Rev. Lett. **78**, 879 (1997).
[11] M. Zepf *et al.*, Phys. Plasmas **3**, 3242 (1996).
[12] J. Fuchs *et al.*, Phys. Rev. Lett. **80**, 2326 (1998).
[13] O. Willi *et al.*, Laser Part. Beams **19**, 5 (2001).
[14] R. Kodama *et al.*, Phys. Plasmas **8**, 2268 (2001).
[15] K. A. Tanaka *et al.*, Phys. Plasmas **7**, 2014 (2000).
[16] Y. Kato, K. Mima, N. Miyanaga, S. Arinaga, Y. Kitagawa, M. Nakatsuka, and C. Yamanaka, Phys. Rev. Lett. **53**, 1057 (1984).
[17] K. A. Tanaka *et al.*, Rev. Sci. Instrum. **76**, 013507 (2005).
[18] H. Takabe *et al.*, Phys. Fluids **31**, 2884 (1988).
[19] K. A. Tanaka, H. Hashimoto, R. Kodama, K. Mima, U. Sentoku, and K. Takahashi, Phys. Rev. E **60**, 3283 (1999).
[20] K. Endo *et al.* (unpublished).
[21] Y. Kitagawa *et al.*, IEEE J. Quantum Electron. **40**, 281 (2004).
[22] J. J. Santos *et al.*, Phys. Rev. Lett. **89**, 025001 (2002).
[23] A. Pukhov, Rep. Prog. Phys. **66**, 47 (2003).
[24] M. H. Key *et al.*, Phys. Plasmas **5**, 1966 (1998).
[25] M. I. K. Santala *et al.*, Phys. Rev. Lett. **84**, 1459 (2000).
[26] R. B. Campbell, R. Kodama, T. A. Mehlhorn, K. A. Tanaka, and D. R. Welch, Phys. Rev. Lett. **94**, 055001 (2005).
[27] Y. Kitagawa *et al.*, Phys. Rev. E **71**, 016403 (2005).